symmetry

IMPACT FACTOR 2.940

CITESCORE 4.3

Article

The Particle-Rotor-Quadrupole-Coupling Model for Transitional Odd-A Nuclei

Aoxue Li, Yingxin Wu, Yu Zhang, Ziwei Feng, Feng Pan and Lianrong Dai

Special Issue

Symmetry in Nuclear Physics: Model Calculations, Advances and Applications

Edited by

Prof. Dr. Jerry Paul Draayer, Dr. Feng Pan and Dr. Andriana Martinou

MDPI

https://doi.org/10.3390/sym14122578

symmetry

Article

The Particle-Rotor-Quadrupole-Coupling Model for Transitional Odd-A Nuclei †

Aoxue Li [1], Yingxin Wu [1], Yu Zhang [1], Ziwei Feng [1], Feng Pan [1,*] and Lianrong Dai [2]

[1] Department of Physics, Liaoning Normal University, Dalian 116029, China
[2] Department of Physics, School of Science, Huzhou University, Huzhou 313000, China
* Correspondence: daipan@dlut.edu.cn
† Dedicated to Jerry P. Draayer in celebration for his 80th birthday.

Abstract: The particle-rotor-quadrupole-coupling model, in which the quadrupole–quadrupole interaction of the even-even core is described by a triaxial rotor with a single-j particle, is adopted to describe low-lying spectra of odd-A nuclei within the vibrational to triaxial transition region. In contrast to the particle-plus-rotor-model, the quadrupole–quadrupole interaction introduced in the particle-rotor-quadrupole-coupling model keeps the rotational symmetry in the collective model framework without approximation. To demonstrate the usability, low-lying level energies, reduced E2 transition probabilities, and ground-state quadrupole moments of ^{135}Ba and ^{131}Xe are fit by the model, of which the results are compared with the experimental data and those of other models. It is shown that the fitting results of the particle-rotor-quadrupole-coupling model to the low-lying level energies, reduced E2 transition probabilities, and ground-state electric quadrupole moments of ^{135}Ba and ^{131}Xe are the best, of which the model parameters of the even-even core are determined by the triaxial rotor model in fitting the low-lying spectra of ^{134}Ba and ^{130}Xe. In comparison with the E(5/4) model results of ^{135}Ba, it is also shown that the quadrupole–quadrupole interaction of the even-even core with the single particle adopted can indeed reproduce the E(5/4) critical point behavior. The fitting quality of the reduced E2 transition probabilities among low-lying states by the particle-rotor-quadrupole-coupling model is also noticeably improved. Thus, it can be concluded that the particle-rotor-quadrupole-coupling model is suitable to describe low-lying properties of odd-A nuclei within the transitional region.

Keywords: triaxial deformation; quadrupole–quadrupole interaction; the particle-rotor-quadrupole-coupling model

PACS: 21.10.Re; 21.60.Ev

check for updates

Citation: Li, A.; Wu, Y.; Zhang, Y.; Feng, Z.; Pan, F.; Dai, L. The Particle-Rotor-Quadrupole-Coupling Model for Transitional Odd-A Nuclei. *Symmetry* **2022**, *14*, 2578. https://doi.org/10.3390/sym14122578

Academic Editor: Charalampos Moustakidis

Received: 8 November 2022
Accepted: 2 December 2022
Published: 6 December 2022

1. Introduction

Until now, it has been shown that both the collective model [1] and the interacting boson model [2] successfully describe low-lying spectra of medium and heavy mass nuclei. In the well-deformed mass region, shell model description based on the pseudo SU(3) model [3–5] has also been proven to be successful [6–8]. Shape (phase) evolution in these nuclei has been extensively studied [9–15].

For odd-mass nuclei, besides the pseudo SU(3) model [16,17], the quadrupole–quadrupole coupling of the even-even core with an odd-particle is adopted in the interacting boson–fermion model (IBFM) [18], while it is treated approximately in the particle-plus-rotor-model (PRM) by using the Nilsson deformed shell model basis for the odd-particle considered [1]. The PRM has been widely used to describe deformed odd-mass nuclei in the collective model framework [19–26]. Nevertheless, though less attention has been paid, multipole interactions of the even-even core with an odd-particle, including the quadrupole–quadrupole interaction, can be considered explicitly without approximation in the collective model framework [27–33].

In this work, the particle-rotor-quadrupole-coupling model (PRQCM)—involving quadrupole–quadrupole interaction of the even-even core with a single-j particle—is adopted to describe low-lying spectra of odd-A nuclei within the vibrational to triaxial transition region. As an example of the model application, low-lying level energies, reduced E2 transition probabilities, and the ground-state quadrupole moments of ^{135}Ba and ^{131}Xe are calculated and compared with the experimental data and the results of the IBFM and the PRM.

2. The Particle-Rotor-Quadrupole-Coupling and Other Models

2.1. The PRQCM Model

Similar to the prescription shown in [27], the Hamiltonian of the PRQCM is expressed as

$$\hat{H} = \hat{H}_{\rm rot} - \kappa\, Q \cdot Q^{\rm F} + b\, \hat{J}^2, \tag{1}$$

where $\hat{H}_{\rm rot}$ is the triaxial rotor Hamiltonian of the even-even core; the second term is the quadrupole–quadrupole interaction of the core with the single particle concerned; and the third term is proportional to the scalar product of the total angular momentum, which is equivalent to the dipole–dipole interaction of the core with the particle introduced in [27]. Since only one particle in a j-orbit is considered, the single-particle energy contribution obtained from the spherical shell model to (1) is merely a constant and not included. The $\hat{H}_{\rm rot}$ is given by

$$\hat{H}_{\rm rot} = \sum_{k=1}^{3} \frac{\hat{L}_k'^{\,2}}{2\Im_k}, \tag{2}$$

where $\hat{L}_k'$ $(k = 1,2,3)$ are the angular momentum operators of the core in the core-fixed intrinsic frame. The three moments of inertia are given by [1]

$$\Im_k = B\beta^2 \sin^2(\gamma - \frac{2\pi k}{3}) \tag{3}$$

for $k = 1,2,3$, where B is the inertia parameter, and β and γ are the deformation and the triaxiality of the rotor, respectively. The quadrupole operator of the core in the laboratory frame can be expressed as

$$Q_\mu = \beta\cos\gamma\, D^{2*}_{\mu 0}(\vartheta_1,\vartheta_2,\vartheta_3) + \frac{\beta\sin\gamma}{\sqrt{2}}\,(D^{2*}_{\mu 2}(\vartheta_1,\vartheta_2,\vartheta_3) + D^{2*}_{\mu -2}(\vartheta_1,\vartheta_2,\vartheta_3)), \tag{4}$$

where $D^{2*}_{\mu\nu}(\vartheta_1,\vartheta_2,\vartheta_3)$ is the Wigner D-function of the Euler angles $\vartheta_1,\vartheta_2,\vartheta_3$ of the rotating core. In the single-j shell model basis, the quadrupole operator of the particle is given by

$$Q^{\rm F}_\mu = \gamma_j\,(a_j^\dagger \times \tilde{a}_j)^2_\mu \tag{5}$$

with

$$\gamma_j = (N_{\rm o} + \frac{3}{2})\,(-1)^{j-\frac{1}{2}}\,\frac{(2j+1)}{\sqrt{20\pi}}\,\langle j\frac{1}{2}, j - \frac{1}{2}|20\rangle, \tag{6}$$

where $a^\dagger_{jm}$ (a_{jm}) is the creation (annihilation) operator of the particle in the single-j orbit with $\tilde{a}_{jm} = (-)^{j+m}a_{j\,-m}$; $N_{\rm o}$ is the number of phonons of the major oscillator shell; and $(a_j^\dagger \times \tilde{a}_j)^2_\mu = \sum_{m_1 m_2}\langle jm_1, jm_2|2\mu\rangle a^\dagger_{jm_1}\tilde{a}_{jm_2}$, in which $\langle jm_1, jm_2|2\mu\rangle$ is the SU(2) Clebsch–Gordan (CG) coefficient.

In the calculation, the Hamiltonian (1) is diagonalized in the coupled basis $\{|(L,j)J\,M_J\,K\rangle\}$, of which the core part is the basis vectors of the triaxial rotor, where $K = 0,2,4,\cdots$ is the quantum number of the core angular momentum projected onto the third axis of the intrinsic frame, L is the angular momentum quantum number of the triaxial rotor with

$$L = \begin{cases} K, K+1, \cdots, & \text{for } K \neq 0, \\ 0, 2, 4, \cdots, & \text{for } K = 0, \end{cases} \tag{7}$$

and J and M_J are the quantum number of the total angular momentum and that of the third component in the laboratory frame, respectively. In the representation of the Euler angles of the core, the corresponding wave function can be written as

$$\begin{aligned} \langle \vartheta_1, \vartheta_2, \vartheta_3 | (L, j) J\, M_J\, K \rangle = \sqrt{\tfrac{2L+1}{16\pi^2}} \sqrt{\tfrac{1}{1+\delta_{K0}}} \textstyle\sum_{M_L m} \langle L M_L, jm | J M_J \rangle \times \\ \left(D^{L\,*}_{M_L\,K}(\vartheta_1, \vartheta_2, \vartheta_3) + (-1)^L D^{L\,*}_{M_L\,-K}(\vartheta_1, \vartheta_2, \vartheta_3) \right) a^{\dagger}_{jm} |0\rangle, \end{aligned} \tag{8}$$

where $|0\rangle$ is the vacuum state of the single-j particle. After diagonalization of the Hamiltonian (1), the eigenstates of (1) are expressed as

$$|J_\alpha M_J\rangle = \sum_{L,K} c^{\alpha}_{L\,K} |(Lj) J\, M_J\, K\rangle,$$

where the expansion coefficients $c^{\alpha}_{L\,K}$ are determined after the diagonalization, and the additional quantum number α labels the α-th eigenstate for given J.

The E2 transition operator is defined as

$$T_\mu = q_2\, (Q_\mu + \xi\, Q^{\mathrm{F}}_\mu), \tag{9}$$

where q_2 is the effective-charge-related parameter, and the dimensionless parameter ξ measures the contribution from the single particle. Thus, the reduced E2 transition probability for the transition $J_\alpha \to J'_{\alpha'}$ and the electric quadrupole moment of the α-th J state $|J_\alpha M_J = J\rangle$ are given by

$$B(E2, J_\alpha \to J'_{\alpha'}) = \frac{2J'+1}{2J+1}\, q_2^2 |\, (\langle J'_{\alpha'} \| Q \| J_\alpha \rangle + \xi\, \langle J'_{\alpha'} \| Q^{\mathrm{F}} \| J_\alpha \rangle)|^2 \tag{10}$$

and

$$Q(J_\alpha) = \sqrt{\frac{16\pi}{5}}\, \langle JJ, 20 | JJ \rangle\, q_2\, (\langle J_\alpha \| Q \| J_\alpha \rangle + \xi\, \langle J_\alpha \| Q^{\mathrm{F}} \| J_\alpha \rangle), \tag{11}$$

respectively, in which the reduced matrix element $\langle J'_{\alpha'} \| T \| J_\alpha \rangle$ is defined in terms of the SU(2) CG coefficient according to the Wigner–Eckart theorem.

2.2. The Particle-Plus-Rotor Model

In contrast to the PRQCM, the particle-plus-rotor model (PRM) has been widely used to describe odd-mass nuclei [19–26]. Actually, the PRM Hamiltonian is the same as that shown in (1) with $\kappa = b = 0$ but with the additional deformed single-particle energy term described in the intrinsic frame:

$$\hat{H} = \hat{H}_{\mathrm{rot}} + \hat{H}_{\mathrm{sp}} \tag{12}$$

with

$$\hat{H}_{\mathrm{sp}} = \pm \frac{1}{2} C \{ \cos\gamma\, (\hat{j}'^{\,2}_0 - \frac{j(j+1)}{3}) + \frac{\sin\gamma}{2\sqrt{3}}\, (\hat{j}'^{\,2}_+ + \hat{j}'^{\,2}_-) \}, \tag{13}$$

where the plus sign refers to a particle and the minus sign to a hole; C is a parameter proportional to the deformation β as adopted in [34–37]; and $\hat{j}'_\mu$ ($\mu = +, -, 0$) are the angular momentum operators of the single particle, which are equivalent to the spherical single-particle energy term plus the quadrupole-coupling of the core with the single-particle term being treated approximately. The single-particle Hamiltonian (13) is digonalized with the eigenstates

$$| \, \nu \rangle = \sum_{\Omega} c^{\nu}_{\Omega} \, |j, \, \Omega \rangle, \quad | \, \bar{\nu} \rangle = \sum_{\Omega} (-1)^{j-\Omega} \, c^{\nu}_{\Omega} \, |j, \, -\Omega \rangle \; , \tag{14}$$

where Ω is the quantum number of the angular momentum of the single particle projected onto the third axis of the intrinsic frame, c^{ν}_{Ω} is determined by the diagonalization of $\hat{H}_{\rm sp}$, and $| \, \bar{\nu} \rangle$ is the time reversal state of $| \, \nu \rangle$. Then, the eigenstates of (12) are expressed in terms of the eigenstates of the total angular momentum coupled to the intrinsic single-particle states as

$$|J_{\alpha} M_J \rangle = \sum_{K,\nu} \Lambda^{\alpha}_{K,\nu} |J \, M_J \, K; \nu \rangle_{\rm S}, \tag{15}$$

where $\{\Lambda^{\alpha}_{K,\nu}\}$ are the expansion coefficients determined by the diagonalization of (12) and

$$|J \, M_J \, K; \, \nu \rangle_{\rm S} = \sqrt{\frac{1}{2}} \Big(|J \, M_J \, K \rangle |\nu \rangle + (-1)^{J-K} |J \, M_J \; - K \rangle |\bar{\nu} \rangle \Big). \tag{16}$$

In the diagonalization process, the angular momentum operators of the core in the core-fixed intrinsic frame $\hat{L}'_k$ are expressed as $\hat{L}'_k = \hat{J}'_k - \hat{j}'_k$, where $\hat{J}'_k$ is the total angular momentum operator in the core-fixed intrinsic frame. Since contribution of the quadrupole moment of the single particle to E2 transitions are very small, the formula of B(E2) values and that of the quadrupole moments shown in (10) and (11) apply to the PRM as well, in which the parameter ξ is simply taken to be zero in the PRM.

2.3. The IBFM Formalism

By comparison with the results of the PRQCM, the IBFM Hamiltonian suitable to describe odd-mass nuclei in the transitional region [38] is also considered, which is expressed in terms of the *s*- and *d*-boson and the single-particle operators as

$$\hat{H}_{\rm IBFM} = \epsilon \, \hat{n}_d - \kappa_0 \, (\hat{Q}^B + \alpha_0 \, q^{\rm F}) \cdot (\hat{Q}^B + \alpha_0 \, q^{\rm F}) + f \hat{L}^2 + g \hat{J}^2, \tag{17}$$

where $\hat{n}_d = \Sigma_{\mu} d^{\dagger}_{\mu} d_{\mu}$ is the *d*-boson number operator; $\hat{Q}^B_{\mu} = d^{\dagger}_{\mu} s + s^{\dagger} \tilde{d}_{\mu}$ is the U(5)-O(6) quadrupole operator of the IBM core; $\hat{q}^{\rm F}_{\mu} = (a^{\dagger}_j \times \tilde{a}_j)^2_{\mu}$; α_0 is a dimensionless parameter; and ϵ, κ_0, f, and g are real model parameters.

The IBFM Hamiltonian (17) is diagonalized in the (U(6) $\supset$ O(6) $\supset$ SO(5) $\supset$ SO(3)) $\otimes$ SU$_j$(2)$\supset$SU$_J$(2) coupled basis

$$|N \, \sigma \, \tau \, \beta \, L; \, j; \, J \, M \rangle = \sum_{M_L m} \langle L M_L, \, jm | J M \rangle a^{\dagger}_{jm} |N \, \sigma \, \tau \, \beta \, L \, M_L \rangle, \tag{18}$$

where $|N \, \sigma \, \tau \, \beta \, L \, M_L \rangle$ is the basis vector of the IBM core labeled under the group chain U(6) $\supset$O(6)$\supset$O(5)$\supset$SO(3) $\supset$SO(2), where N is the total number of bosons, σ is the O(6) seniority number, τ is the *d*-boson seniority number, and β is an additional quantum number needed in the reduction O(5)$\downarrow$O(3).

After diagonalization of (17), the eigenstates of the IBFM Hamiltonian can be expressed as

$$|J_{\alpha} \, M_J \rangle_{\rm IBFM} \equiv |N, \, j; \, J_{\alpha} \, M_J \rangle = \sum_{\sigma\tau\beta L} C^{\alpha,J}_{\sigma\tau\beta L} |N \, \sigma \, \tau \, \beta \, L; \, j; \, J \, M_J \rangle, \tag{19}$$

where $C^{\alpha,J}_{\sigma\tau\beta L}$ is determined by the diagonalization. Similar to (9), the E2 operator is defined as

$$T^{\rm IBFM}_{\mu} = \tilde{q}_2 \, (\hat{Q}^B_{\mu} + \alpha_0 \, \hat{q}^F_{\mu}). \tag{20}$$

Therefore, the reduced E2 transition probability for the transition $J_\alpha \to J'_{\alpha'}$ and the electric quadrupole moment of the state $|J_\alpha M_J = J\rangle_{\mathrm{IBFM}}$ are still given by (10) and (11) with replacement of the matrix element of T_μ by the matrix element of T_μ^{IBFM} between the eigenstates shown in (19).

3. Model Fit to ^{135}Ba and ^{131}Xe

To demonstrate the applicability of the PRQCM, low-lying level energies, reduced E2 transition probabilities, and the ground-state quadrupole moments of ^{135}Ba and ^{131}Xe are fit. Since there is no β- and γ-vibration in the triaxial rotor model, the core parameters of ^{135}Ba and ^{131}Xe are determined in fitting to the ground-state band and γ-band level energies of the adjacent even-even nuclei ^{134}Ba and ^{130}Xe, respectively. Specifically, the core parameters of both the PRQCM (1) and the PRM Hamiltonian (17) are $\frac{\hbar^2}{B}$ = 65 keV, γ = 30°, $\beta = -0.127$, and b = 15 keV for ^{134}Ba, while $\frac{\hbar^2}{B}$ = 77 keV, γ = 40°, $\beta = -0.127$, and b = 5 keV for ^{130}Xe, where the deformation β is determined by $\beta = \frac{4}{3}\sqrt{\frac{\pi}{5}}\varepsilon_2$ with $\varepsilon_2 = -0.12$ taken from [39]. The fitting results of the level energies of ^{134}Ba and ^{130}Xe are shown in Table 1, in which the IBM results are also shown. The parameters of the IBM Hamiltonian are ϵ = 420.00 keV, κ_0 = 2.65 keV, $f + g$ = 14.69 keV for ^{134}Ba, and ϵ = 415.00 keV, κ_0 = 2.30 keV, $f + g$ = 20.43 keV for ^{130}Xe, where the values of f, g, and α_0 are further determined in fitting to the level energies of ^{135}Ba or ^{131}Xe.

After the model parameters of the core are fixed, the effective-charge-related parameter q_2 in the triaxial rotor model and $\tilde{q}_2$ in the IBM are determined in fitting to B(E2;$2_1^+ \to 0_g^+$), which yields $q_2 = 109.4234\ \sqrt{\mathrm{W.u.}}$ and $138.1106\ \sqrt{\mathrm{W.u.}}$ for ^{134}Ba and ^{130}Xe, respectively, and yields $\tilde{q}_2 = 5.0584\ \sqrt{\mathrm{W.u.}}$ and $5.287\ \sqrt{\mathrm{W.u.}}$ for ^{134}Ba and ^{130}Xe, respectively, in the IBM. Table 2 shows some B(E2) values of ^{134}Ba and ^{130}Xe with the effective-charge-related parameter fixed, in which only experimentally known values fitted by the models are provided.

Table 1. Low-lying level energies (in MeV) below 2.211 (2.172) MeV in the ground-state band and γ-band of ^{134}Ba (^{130}Xe) fitted by the triaxial rotor model (this work) and the IBM, where the spin and parity of the 7-th level of ^{134}Ba (^{130}Xe) is 4^+ (5^+).

L_α^π	^{134}Ba [40]	This Work	IBM	^{130}Xe [41]	This Work	IBM
0_g^+	0	0	0	0	0	0
2_1^+	0.605	0.504	0.665	0.536	0.385	0.672
2_2^+	1.168	0.801	1.070	1.122	0.925	1.074
3_1^+	1.643	1.305	1.525	1.643	1.305	1.525
4_1^+	1.401	1.479	1.227	1.205	1.155	1.261
4_2^+	1.970	2.302	1.613	1.808	1.921	1.645
4_3^+ (5_1^+)	2.118	2.744	1.993	2.172	2.192	2.224
6_1^+	2.211	2.871	1.868	1.944	2.263	1.947

Table 2. Some B(E2;$L_\alpha \to L'_\alpha$) values (in W.u.) of ^{134}Ba and ^{130}Xe, where only experimentally known values of the intra- and inter-band transitions of the ground-state band and γ band fitted by the models are shown, and * indicates that the corresponding experimental value is exactly fit in determining the effective-charge-related parameter q_2 or $\tilde{q}_2$.

	^{134}Ba [40]	This Work	IBM		^{130}Xe [41]	This Work	IBM
$2_1^+ \to 0_g^+$	33.6(6)	33.6 *	33.6 *	$2_1^+ \to 0_g^+$	38(5)	38 *	38 *
$4_1^+ \to 2_1^+$	52(6)	47.02	47.32	$4_1^+ \to 2_1^+$	>0.054	71.7	34.09
$4_1^+ \to 2_2^+$	0.16(16)	0.42	0.32	$6_1^+ \to 4_1^+$	>0.033	84.6	47.70
$2_2^+ \to 0_g^+$	0.42(13)	0.10	0.11	$2_2^+ \to 2_1^+$	>0.056	19.6	1.77
$2_2^+ \to 2_1^+$	73(22)	44.03	43.41	$5_2^+ \to 6_1^+$	13(3)	1.90	15.22
$3_1^+ \to 2_2^+$	4.3(12)	1.97	3.51	$5_2^+ \to 3_1^+$	0.0017(13)	3.92	8.20
$3_1^+ \to 2_1^+$	0.024(8)	0.18	0.02				

We then use the model Hamiltonian (1) with the above parameters of the core to fit level energies of ^{135}Ba and ^{131}Xe to determine the quadrupole–quadrupole interaction strength κ, of which the fitting results are presented in Table 3 for the level energies below 2.283 MeV for ^{135}Ba and Table 4 for the level energies below 1.621 MeV for ^{131}Xe, respectively. The best fit yields $\kappa = 3.115$ (0.257) MeV for ^{135}Ba (^{131}Xe). It should be noted that $\kappa|\beta|\cos\gamma$ and $q_2|\beta|\cos\gamma$ are compatible with the IBFM parameters κ_0 and $\tilde{q}_2$, respectively, although a relatively larger value of κ is needed for ^{135}Ba. In Tables 3 and 4, the IBFM and the PRM results are also presented for comparison. For the IBFM, the best fit yields $\alpha_0 = 0.8$ (1.3), $f = 3.85$ (7.54) keV, and $g = 10.84$ (12.89) keV for ^{135}Ba (^{131}Xe). The PRM parameter $C = 0.3$ (0.1) MeV for ^{135}Ba (^{131}Xe) is taken. In Table 3, the E(5/4) model fitting results [42] of ^{135}Ba are also shown for comparison since ^{135}Ba is often considered to be the E(5/4) critical point candidate of the U(5) (vibration) to O(6) (γ-soft) shape phase transition [38,43].

Table 3. Low-lying level energies (in MeV) below 2.283 MeV of ^{135}Ba and below 1.621 MeV of ^{131}Xe fitted by the PRQCM (this work), where the spin and parity of the levels with the level energy underlined is not determined in experiments [44,45], and "–" indicates the level is not calculated in the E(5/4) model [42].

J^π_α	^{135}Ba [45]	This Work	IBFM	PRM	E(5/4) [42]	^{131}Xe [44]	This Work	IBFM	PRM
$3/2^+_g$	0	0	0	0	0	0	0	0	0
$3/2^+_2$	0.588	0.414	0.600	0.480	0.613	0.405	0.355	0.595	0.281
$3/2^+_3$	0.855	0.711	1.005	0.750	0.683	0.700	0.895	0.996	0.986
$3/2^+_4$	1.214	1.125	1.374	1.230	0.989	0.994	1.250	1.357	1.267
$1/2^+_1$	0.221	0.334	0.567	0.375	0.228	0.080	0.332	0.556	0.315
$1/2^+_2$	0.910	0.701	0.972	0.855	0.901	0.565	0.888	0.958	0.952
$5/2^+_1$	0.481	0.350	0.654	0.331	0.569	0.364	0.386	0.659	0.293
$5/2^+_2$	0.980	0.925	1.060	0.749	0.901	0.723	0.914	1.060	1.021
$5/2^+_3$	1.238	1.200	1.063	0.974	1.208	1.034	1.076	1.066	1.220
$5/2^+_4$	1.557	1.366	1.449	1.185	1.251	1.245	1.275	1.449	1.510
$5/2^+_5$	1.941	2.054	1.737	2.094	1.663				
$5/2^+_6$	2.075	2.430	1.816	2.542	–				
$7/2^+_1$	0.875	0.625	0.730	0.427	0.875	0.637	0.413	0.750	0.281
$7/2^+_2$	1.008	0.860	1.135	0.802	1.199	0.973	0.957	1.151	0.826
$7/2^+_3$	1.130	1.305	1.140	1.053	1.514	0.952	1.117	1.158	0.977
$7/2^+_4$	1.165	1.311	1.525	1.178	1.558	1.621	1.310	1.543	1.262
$9/2^+_1$	1.200	1.384	1.238	1.001	1.593	0.971	1.164	1.274	0.808
$9/2^+_2$	2.283	1.440	1.622	1.197	1.899	1.456	1.355	1.660	1.256
$11/2^+_1$	1.955	1.718	1.742	1.028	2.065	1.397	1.213	1.414	0.841
$13/2^+_1$						1.584	2.266	2.018	1.594
$\sigma(E)$ (MeV)		0.271	0.251	0.413	0.276		0.254	0.294	0.277

It should be pointed out that spin and parity of several levels in both ^{135}Ba and ^{131}Xe with the level energy underlined shown in Table 3 have not been determined in experiments. If the spin and parity of the levels with the underlined level energy shown in Table 3 are indeed as predicted in all three models, there is one-to-one correspondence of the experimental level energy below 2.283 MeV in ^{135}Ba and 1.621 MeV in ^{131}Xe, respectively, to that predicted by the three models.

Table 4. Some B(E2;$J_\alpha \to J'_\alpha$) (in W.u.) values of ^{135}Ba and ^{131}Xe, where "–" indicates the corresponding value is not available experimentally or is not calculated in the E(5/4) model [42].

	^{135}Ba [45]	**This Work**	**IBFM**	**PRM**	**E(5/4) [42]**		**^{131}Xe [44]**	**This Work**	**IBFM**	**PRM**
$1/2_1^+ \to 3/2_g^+$	4.6(2)	14.80	19.09	38.52	17.43	$1/2_1^+ \to 3/2_g^+$	<37	36.70	17.82	41.26
$5/2_1^+ \to 1/2_1^+$	2.6(5)	3.80	0.19	0.94	–	$5/2_1^+ \to 1/2_1^+$	7.64(24)	7.68	0.39	4.55
$5/2_1^+ \to 3/2_g^+$	28.3(10)	32.60	13.02	38.21	18.81	$5/2_1^+ \to 3/2_g^+$	27.8(9)	38.80	14.10	68.30
$7/2_1^+ \to 3/2_2^+$	<1.0	1.47	0.11	0.44	–	$7/2_1^+ \to 3/2_2^+$	1.52(25)	4.39	0.35	6.78
$7/2_1^+ \to 5/2_1^+$	12.8(12)	9.40	0.32	1.96	–	$7/2_1^+ \to 5/2_1^+$	1.6(13)	11.50	0.68	26.39
$7/2_1^+ \to 3/2_g^+$	19.9(8)	31.00	2.60	37.01	19.9	$7/2_1^+ \to 3/2_g^+$	22.2(19)	37.70	3.10	52.31
$1/2_2^+ \to 3/2_g^+$	11.7(10)	1.62	0.41	0	–	$1/2_2^+ \to 3/2_g^+$	10(6)	12.00	1.08	6.28
$3/2_2^+ \to 1/2_1^+$	–	2.48	0.01	0	–	$3/2_2^+ \to 1/2_1^+$	24(+26 −24)	20.50	0.02	30.80
$3/2_2^+ \to 3/2_g^+$	18.0(10)	33.60	0.18	23.49	–	$3/2_2^+ \to 3/2_g^+$	30	38.00	0.42	50.22
$5/2_2^+ \to 1/2_1^+$	–	9.30	0.77	13.40	14.8	$5/2_2^+ \to 1/2_1^+$	25.7(25)	1.61	0.62	52.63
$5/2_2^+ \to 5/2_1^+$	–	2.01	1.32	6.93	4.0	$5/2_2^+ \to 5/2_1^+$	–	0.88	1.32	4.81
$5/2_2^+ \to 7/2_1^+$	–	8.90	3.83	20.48	6.69	$5/2_2^+ \to 7/2_1^+$	–	10.01	3.24	0.43
$9/2_1^+ \to 7/2_1^+$	–	9.85	4.39	10.91	6.63	$9/2_1^+ \to 7/2_1^+$	–	15.40	3.70	19.13
$3/2_3^+ \to 1/2_1^+$	–	15.30	4.90	19.26	8.40	$5/2_2^+ \to 3/2_2^+$	4(+6 −4)	7.97	3.00	25.30
$3/2_3^+ \to 5/2_1^+$	–	15.11	5.10	29.18	13.47	$5/2_2^+ \to 3/2_g^+$	4.8(5)	9.86	0.04	0.34
$3/2_3^+ \to 7/2_1^+$	–	9.04	0.88	6.17	2.95	$7/2_2^+ \to 3/2_g^+$	1.6(7)	11.0	0.17	0.56
$3/2_3^+ \to 3/2_g^+$	7.0(10)	0.10	0.31	0	–					
σ(B(E2))		9.02	12.45	14.44	16.34			10.24	15.59	19.39

The fitting quality is measured by the rms deviation of the level energies defined as

$$\sigma(E) = \sqrt{\frac{1}{n_0 - n_m} \sum_{i=1}^{n_0} |E^i_{\rm th} - E^i_{\rm exp}|^2}, \tag{21}$$

where n_0 is the total number of level energies fitted with $n_0 = 18$ (17) for ^{135}Ba (^{131}Xe); n_m is the number of model parameters with $n_m = 1$ in the PRQCM and the PRM; $n_m = 2$ in the IBFM; $n_m = 5$ in the E(5/4) model [42] for ^{135}Ba, because other model parameters have already been determined in the fitting to the level energies of the even-even nuclei; and $E^i_{\rm exp}$ and $E^i_{\rm th}$ are experimental and theoretical level energies. It is clearly shown that the fitting quality of the three models is quite the same. Nevertheless, as far as the level energies of ^{135}Ba and ^{131}Xe shown in Table 3 are concerned, the average values of the rms deviation of ^{135}Ba and that of ^{131}Xe in the PRQCM, the IBFM, and the PRM fit are $\overline{\sigma}(E) = 0.263$, 0.273, and 0.345, respectively, indicating that the fitting quality of the PRQCM is the best. The average level energy deviation in the PRM is the largest, which may be due to the fact that the quadrupole-coupling is approximately treated.

By using the model parameters shown above and the effective charge parameter q_2 in the PRQCM or the PRM and $\tilde{q}_2$ in the IBFM from fitting to the B(E2;$2_1^+ \to 0_g^+$) of ^{134}Ba and ^{130}Xe, the B(E2) values of the transitions between the states with the level energies shown in Table 3 are calculated. The best fit yields the additional parameter $\xi = -0.0104$ (-0.0025) of the PRQCM for ^{135}Ba (^{131}Xe), which shows that the contributions of the quadrupole moment of the single particle to the total E2 transition operators are indeed small. The E(5/4) model results presented in [42] are also included in Table 3 for comparison. The fitting deviation from the experimental B(E2) values is defined the same as that shown in (21), with the level energies replaced by the B(E2) values also being calculated. Since the effective charge q_2 or $\tilde{q}_2$ has already been determined in fitting the B(E2) values of the even-even nuclei, $n_m = 1$ in the PRQCM, $n_m = 2$ in the E(5/4) model [42], and $n_m = 0$ in both the PRM and the IBFM in calculating the corresponding rms deviations. It is clearly shown in Table 4 that the fitting quality of the PRQCM is the best. The average values of the rms deviation in B(E2) values of ^{135}Ba and that of ^{131}Xe in the PRQCM, the IBFM, and the PRM fit are $\overline{\sigma}$(B(E2)) $= 9.63$, 14.02, 16.92, respectively. The calculated results of the low-lying level energies of ^{135}Ba and ^{131}Xe with some reduced E2 transition rates in comparison to the experimental ones are shown in Figures 1 and 2, respectively.

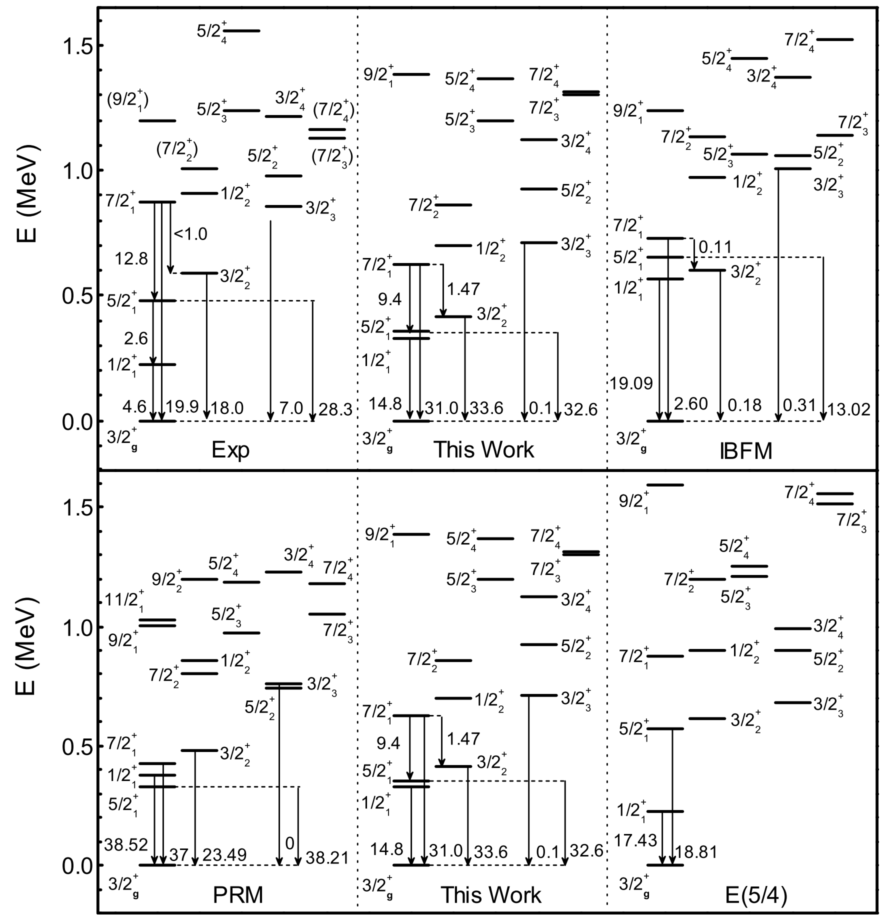

Figure 1. The low-lying spectrum of ^{135}Ba and some reduced E2 transition rates, where the Exp part provides the experimental results [45]. The upper panel shows the comparison of the results of this work with the experimental ones and those of the IBFM, while the lower panel shows the comparison of the results of this work with those of the PRM and the E(5/4) model [42].

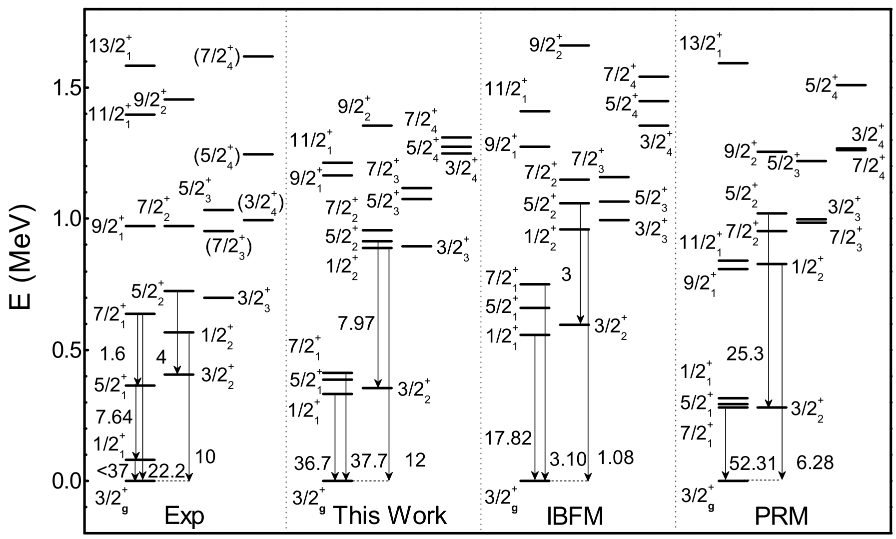

Figure 2. The low-lying spectrum of ^{131}Xe and some reduced E2 transition rates, where the Exp part provides the experimental results [44].

Since the electric quadrupole moments of ^{134}Ba and ^{130}Xe, and those of excited states of ^{135}Ba and ^{131}Xe are not available experimentally, only the ground-state electric quadrupole moment $Q(3/2^+_g)$ of ^{135}Ba and ^{131}Xe are calculated, which are provided in Table 5. It can be seen that the PRQCM results of the ground-state electric quadrupole moments of ^{135}Ba and ^{131}Xe are closest to the experimental values, although the sign of the ground-state electric quadrupole moment of ^{131}Xe obtained from the PRQCM is still incorrect.

Table 5. The ground-state electric quadrupole moment $Q(3/2^+_g)$ (in eb) of ^{135}Ba and ^{131}Xe.

^{135}Ba [45]	This work	IBFM	PRM
+0.160(3)	+0.187	+0.075	+0.412
^{131}Xe [44]	This work	IBFM	PRM
−0.114(1)	+0.055	+0.126	+0.276

4. Summary

In this work, the particle-rotor-quadrupole-coupling model—involving the quadrupole–quadrupole interaction of the even-even core described by a triaxial rotor with a single-j particle—is adopted to describe low-lying spectra of odd-A nuclei within the vibrational to triaxial transition region. To demonstrate the usability, the low-lying level energies, reduced E2 transition probabilities, and ground-state quadrupole moments of ^{135}Ba and ^{131}Xe are fit by the model, of which the results are compared with the experimental data and those of other models. It is shown that the fitting results of the particle-rotor-quadrupole-coupling model to the low-lying level energies, reduced E2 transition probabilities, and ground-state electric quadrupole moments of ^{135}Ba and ^{131}Xe are the best, of which the model parameters of the even-even core are determined by the triaxial rotor model in fitting to the low-lying spectra of ^{134}Ba and ^{130}Xe. In comparison with the E(5/4) model results of ^{135}Ba, it is also shown that the quadrupole–quadrupole interaction of the even-even core with the single particle adopted can indeed reproduce the E(5/4) critical point behavior. The fitting quality of the reduced E2 transition probabilities among the low-lying states by the particle-rotor-quadrupole-coupling model is also noticeably improved. Thus, it can be concluded that the particle-rotor-quadrupole-coupling model is suitable to describe low-lying properties of odd-A nuclei within the transitional region.

To improve the present model for odd-mass nuclei, a model Hamiltonian including the γ-unstable motion initiated by Wilets and Jean for transitional nuclei or that of the rotor–vibrator with an axially deformed shape for well-deformed nuclei may be adopted to replace the triaxial rotor for the even-even core in the collective model framework. Extension of the model to inclusion of multi-j, single-particle orbits is also possible. These possible extensions and improvements may be considered in our future work.

Author Contributions: Methodology, F.P.; numerical calculations and analyses, A.L., Y.W., Y.Z., Z.F., and L.D.; writing–original draft and editing, F.P.; senior leadership and oversight, F.P. All authors have read and agreed to the final version of the manuscript.

Funding: This research was funded by the National Natural Science Foundation of China (12175097, 12175066).

Institutional Review Board Statement: Not applicable.

Informed Consent Statement: Not applicable.

Data Availability Statement: The Mathematica code for the model calculation and the results presented are available upon request.

Conflicts of Interest: The authors have no conflict of interest.

References

1. Bohr, A.; Mottelson, B.R. Nuclear Structure II (Benjamin, Reading, 1975). Available online: https://books.google.com/books?hl=zh-CN&lr=&id=NNZQDQAAQBAJ&oi=fnd&pg=PP1&ots=yXMnYGlZ-d&sig=6Rb4Iz36-HozG5O0_-luO_gxvzo (accessed on 1 November 2022).
2. Iachello, F.; Arima, A. *The Interacting Boson Model*; Cambridge University: Cambridge, UK, 1987. Available online: https://books.google.com/books/about/The_Interacting_Boson_Model.html?id=fB7Qe73VmsgC (accessed on 1 November 2022).
3. Draayer, J.P.; Weeks, K.J. Shell-model description of the low-energy structure of strongly deformed nuclei. *Phys. Rev. Lett.* **1983**, *51*, 1422–1425. [CrossRef]
4. Draayer, J.P.; Weeks, K.J. Towards a shell model description of the low-energy structure of deformed nuclei I. Even-even systems. *Ann. Phys.* **1984**, *156*, 41–47. [CrossRef]
5. Castaños, O.; Draayer, J.P.; Laschber, Y. Towards a shell-model description of the low-energy structure of deformed nuclei II. Electromagnetic properties of collective M1 bands. *Ann. Phys.* **1987**, *180*, 290–329. [CrossRef]
6. Rompf, D.; Beuschel, T.; Draayer, J.P.; Scheid, W.; Hirsch, J.G. Towards understanding magnetic dipole excitations in deformed nuclei: Phenomenology. *Phys. Rev. C* **1998**, *57*, 1703–1718. [CrossRef]
7. Beuschel, T.; Hirsch, J.G.; Draayer, J.P. Scissors mode and the pseudo-SU(3) model. *Phys. Rev. C* **2000**, *61*, 054307. [CrossRef]
8. Popa, G.; Hirsch, J.G.; Draayer, J.P. Shell model description of normal parity bands in even-even heavy deformed nuclei. *Phys. Rev. C* **2000**, *62*, 064313. [CrossRef]
9. Nikšić, T.; Vretenar, D.; Lalazissis, G.A.; Ring, P. Microscopic description of nuclear quantum phase transitions. *Phys. Rev. Lett.* **2007**, *99*, 092502. [CrossRef]
10. Casten, R.F. Quantum phase transitions and structural evolution in nuclei. *Prog. Part. Nucl. Phys.* **2009**, *62*, 183–209. [CrossRef]
11. Cejnar, P.; Jolie, J.; Casten, R.F. Quantum phase transitions in the shapes of atomic nuclei. *Rev. Mod. Phys.* **2010**, *82*, 2155–2212. [CrossRef]
12. Budaca, R.; Buganu, P.; Budaca, A.I. Bohr model description of the critical point for the first order shape phase transition. *Phys. Lett. B* **2018**, *776*, 26–31. [CrossRef]
13. Fortunato, L. Quantum phase transitions in algebraic and collective models of nuclear structure. *Prog. Part. Nucl. Phys.* **2021**, *121*, 103891. [CrossRef]
14. Böyükata, M.; Alonso, C.E.; Arias, J.M.; Fortunato, L.; Vitturi, A. Review of shape phase transition studies for Bose-Fermi systems: the effect of the odd-particle on the bosonic core. *Symmetry* **2021**, *13*, 215. [CrossRef]
15. Majarshin, A.J.; Luo, Y.-A.; Pan, F.; Fortune, H.T.; Zhang, Y.; Draayer, J.P. Quantum phase transitions and band mixing in ^{135}Ba. *J. Phys. G Nucl. Part Phys.* **2021**, *48*, 125107. [CrossRef]
16. Weeks, K.J.; Draayer, J.P. Shell-model predictions for unique parity yrast configurations of odd-mass deformed nuclei. *Nucl. Phys. A* **1983**, *393*, 69–94. [CrossRef]
17. Naqvi, H.A.; Bahri, C.; Troltenier, D.; Draayer, J.P.; Faessler, A. Algebraic realization of the quantum rotor-odd-A nuclei. *Z. Phys. A* **1995**, *351*, 259–270. [CrossRef]
18. Iachello, F.; Van Isacker, P. *The Interacting Boson-Fermion Model*; Cambridge University: Cambridge, UK, 1991. Available online: https://books.google.com/books?hl=zh-CN&lr=&id=P5fOgnA6xF8C&oi=fnd&pg=PP1&dq=interacting+boson+fermion+model&ots=mDTaEptRgt&sig=dJyiyrYVCMPz0kY6yNUQipQgmY0 (accessed on 1 November 2022).
19. Meyer-Ter-Vehn, J. Collective model description of transitional odd-A nuclei (I). The triaxial-rotor-plus-particle model. *Nucl. Phys. A* **1975**, *249*, 111–140. [CrossRef]
20. Meyer-Ter-Vehn, J. Collective model description of transitional odd-A nuclei (II). Comparison with unique parity states of nuclei in the A=135 and A=190 mass. *Nucl. Phys. A* **1975**, *249*, 141–165. [CrossRef]
21. Toki, H.; Faessler, A. Asymmetric rotor model for decoupled bands in transitional odd-mass nuclei. *Nucl. Phys. A* **1975**, *253*, 231–252. [CrossRef]
22. Hilton, R.R.; Mang, H.J.; Ring, P.; Egido, J.L.; Herold, H.; Reinecke, M.; Ruder, H.; Wunner, G. On the particle-plus-rotor model. *Nucl. Phys. A* **1981**, *366*, 365–383. [CrossRef]
23. Zhang, S.Q.; Qi, B.; Wang, S.Y.; Meng, J. Chiral bands for a quasi-proton and quasi-neutron coupled with a triaxial rotor. *Phys. Rev. C* **2007**, *75*, 044307. [CrossRef]
24. Hamamoto, I. Wobbling excitations in odd-A nuclei with high-j aligned particles. *Phys. Rev. C* **2002**, *65*, 044305. [CrossRef]
25. Quan, S.; Liu, W.P.; Li, Z.P.; Smith, M.S. Microscopic core-quasiparticle coupling model for spectroscopy of odd-mass nuclei. *Phys. Rev. C* **2017**, *96*, 054309. [CrossRef]
26. Chen, Q.B.; Lv, B.F.; Petrache, C.M.; Meng, J. Multiple chiral doublets in four-j shells particle rotor model: Five possible chiral doublets in $^{136}_{60}$Nd$_{76}$. *Phys. Lett. B* **2018**, *782*, 744–749. [CrossRef]
27. De-Shalit, A. Core excitations in nondeformed, Odd-A, nuclei. *Phys. Rev.* **1961**, *122*, 1530–1536. [CrossRef]
28. Thankappan, V.K.; True, W.W. Properties of the low-lying Cu^{63} levels. *Phys. Rev.* **1965**, *137*, B793–B799. [CrossRef]
29. Stein, N.; Whitten, C.A., Jr.; Bromley, D.A. Particle-core coupling in the lead nuclei. *Phys. Rev. Lett.* **1968**, *20*, 113–117. [CrossRef]
30. Hoffman-Pinther, P.; Adams, J.L. ^{90}Y in the core-coupling model. *Nucl. Phys. A* **1974**, *229*, 365–386. [CrossRef]
31. Tanaka, Y.; Sheline, R.K. Comparison of caculated and experimental band structure in odd-A nuclei with A=187–199. *Nucl. Phys. A* **1977**, *276*, 101–118. [CrossRef]

32. Abecasis, S.M.; Davidson, J.; Davidson, M. Particle-core coupling model applied to ^{89}Y, ^{87}Sr, and ^{89}Sr. *Phys. Rev. C* **1980**, *22*, 2237–2242. [CrossRef]
33. Oros-Peusquen, A.M.; Mantica, P.F. Particle-core coupling around ^{68}Ni: A study of the subshell closure at N = 40. *Nucl. Phys. A* **2000**, *669*, 81–100. [CrossRef]
34. Peng, J.; Meng, J.; Zhang, S.Q. Description of chiral doublets in A∼130 nuclei and the possible chiral doublets in A∼100 nuclei. *Phys. Rev. C* **2003**, *68*, 044324. [CrossRef]
35. Qi, B.; Zhang, S.Q.; Meng, J.; Wang, S.Y.; Frauendorf, S. Chirality in odd-A nucleus ^{135}Nd in particle rotor model. *Phys. Lett. B* **2009**, *675*, 175–180. [CrossRef]
36. Wang, S.Y.; Zhang, S.Q.; Qi, B.; Meng, J. Doublet bands in ^{126}Cs in the triaxial rotor model coupled with two quasiparticles. *Phys. Rev. C* **2007**, *75*, 024309. [CrossRef]
37. Qi, B.; Zhang, S.Q.; Meng, J.; Wang, S.Y.; Koike, T. Chirality in odd-A Rh isotopes within the triaxial particle rotor model. *Phys. Rev. C* **2011**, *83*, 034303. [CrossRef]
38. Caprio, M.A.; Iachello, F. Analytic descriptions for transitional nuclei near the critical point. *Nucl. Phys. A* **2007**, *781*, 26–66. [CrossRef]
39. Möller, P.; Sierk, A.J.; Ichikawa, T.; Sagawa, H. Nuclear ground-state masses and deformations: FRDM (2012). *At. Data Nucl. Data Tables* **2016**, *109*, 1–204. [CrossRef]
40. Sonzogni, A.A. Nuclear data sheets for A = 134. *Nucl. Data Sheets* **2004**, *103*, 1–182. [CrossRef]
41. Singh, B. Nuclear data sheets for A = 130. *Nucl. Data Sheets* **2001**, *93*, 33–242. [CrossRef]
42. Inci, I. Investigation of γ-unstable odd-even nuclei in the collective model framework with the Morse potential. *Nucl. Phys. A* **2019**, *991*, 121611. [CrossRef]
43. Alonso, C.E.; Arias, J.M.; Vitturi, A. Critical-point symmetries in boson-fermion systems: The case of shape transitions in odd nuclei in a multiorbit model. *Phys. Rev. Lett.* **2007**, *98*, 052501. [CrossRef]
44. Khazov, Y.; Mitropolsky, I.; Rodionov, A. Nuclear data sheets for A = 131. *Nucl. Data Sheets* **2006**, *107*, 2715–2930. [CrossRef]
45. Singh, B.; Rodionov, A.A.; Khazov, Y.L. Nuclear data sheets for A = 135. *Nucl. Data Sheets* **2008**, *109*, 517–698. [CrossRef]